



Analysis of the Microstructure Formation Process and Its Influence on the Performance of Polymer Electrolyte Fuel-Cell Catalyst Layers

Shinichi Takahashi, Tetsuya Mashio, Norifumi Horibe, Ken Akizuki, and Atsushi Ohma*^[a]

To understand the formation process of the microstructure of the catalyst layer of a polymer electrolyte fuel cell (PEFC), we tried to observe the “real” structure of the catalyst ink by cryogenic scanning electron microscopy (cryo-SEM). Catalyst inks with different water/alcohol compositions were successfully visualized, and they correlated well with the particle-size distribution obtained by laser diffraction of the ink and the structures of the catalyst layers obtained by typical SEM. On the basis of other electrochemical characterization results, includ-

ing current–voltage performance, oxygen reduction reaction kinetics, and mass-transport properties, the microstructures of the catalyst inks and the catalyst layers were proposed. The proposed microstructures can explain the relationship between the catalyst materials and the performance of the cathode catalyst layer of the membrane electrode assembly through its formation and apparent properties. It was also found that the microstructure of the catalyst ink plays an important role in performance.

1. Introduction

Global warming is one of the biggest social issues of the future, and it is mainly caused by the emission of carbon dioxide (CO₂). The development of technologies to reduce the emission of CO₂ is important to auto manufacturers, and Nissan has been developing zero-emission vehicles such as battery electric vehicles and fuel-cell electric vehicles. The biggest issues precluding entry of fuel-cell electric vehicles into the market are cost reduction of polymer electrolyte fuel cell (PEFC) power systems, including hydrogen-storage subsystems, and the development of hydrogen infrastructure. Related to the former issue, one of the most significant challenges is to reduce a platinum-group metal in the fuel-cell stack, as it is used as an electrocatalyst in the catalyst layers of membrane electrode assemblies (MEAs).


Various kinds of research activities on PEFC electrocatalysts have been reported, and high oxygen reduction reaction (ORR) activity and durability are mainly measured in aqueous electrolyte systems such as by the rotating disk electrode method.^[1–8] On the other hand, an electrocatalyst is mixed with an electrolyte to form catalyst layers through deposition and solidification processes. From an industrial point of view, the performance of the electrocatalyst must be guaranteed as a catalyst layer of a MEA. The catalyst layer is a multiscale component, that is, a microscale porous electrode consisting of nanoscale materials, at which an electrochemical reaction and mass transport occur simultaneously. The micro- and nanostructures of catalyst layers have been gradually revealed by means of

characterization techniques that have progressed recently, such as electron microscopy.^[9,10] However, from an industrial design aspect, it is still necessary to characterize the microstructure and the properties of catalyst layers as average values.

To rationally design the catalyst layer for further platinum group metal reduction, so far we have been conducting research on catalyst layers based on a strategy to understand the correlation between catalyst layer performance and the applied materials through the apparent properties and structure by a key mechanism.^[11] Regarding the properties, gas-transport resistance in catalyst layers has been analytically measured with reasonable interpretation,^[12–14] consistent with the results from other research activities.^[15,16] Proton-transport resistance in catalyst layers has been analyzed by electrochemical impedance spectroscopy.^[17,18] We also proposed a unique method involving the use of a hydrogen pump technique to understand the proton-transport phenomenon.^[19,20] With regard to the microstructure of the catalyst layer, we found that ionomer coverage on the electrocatalyst can be a key parameter governing the properties of the catalyst, and this can be done by quantifying the ionomer coverage on platinum and by studying the correlation to the apparent kinetic properties of the catalyst layers.^[21,22]

Regarding process analysis of the catalyst layer, the influence of materials and/or process parameters such as solvent have been studied.^[23–31] However, the results showed the correlation between the materials and the process as input and the current–voltage (*I*–*V*) performance as output, and detailed analysis on the process was not conducted from microstructure and electrochemical properties aspects. Besides, the structure and electrochemical properties of the catalyst layer were not so characterized. On the other hand, some research activities

[a] Dr. S. Takahashi, T. Mashio, N. Horibe, K. Akizuki, A. Ohma
Research Division, Nissan Motor Co., Ltd.,
1, Natsushima, Yokosuka, Kanagawa (Japan), 237-8523
E-mail: a-ohma@mail.nissan.co.jp

 An invited contribution to a Special Issue on In Situ Monitoring of Fuel Cell and Battery Processes

have focused on structure formation in the catalyst ink and have provided new insight into ionomer adsorption/desorption behavior on the catalyst materials.^[32–34] However, they do not mention any relation with the performance of the catalyst layer.

In this report, we try to understand microstructure formation of the catalyst layer by using a “real” catalyst ink, an intermediate state from the materials to catalyst layer formation. The microstructure of the catalyst ink was observed by using cryogenic scanning electron microscopy (cryo-SEM). Because solvent composition of the catalyst ink affects the performance of the catalyst layers of the MEAs,^[28–30] the effect of solvent on the ink structure was first observed by cryo-SEM and was evaluated by laser diffraction. Then, the results were correlated with the electrochemical properties of the catalyst layers to finally propose the microstructure of the ionomer around the electrocatalyst.

Experimental Section

Preparation and Deposition of the Catalyst Ink

Table 1 shows the MEA specifications for this study. A typical platinum-based electrocatalyst (TEC10E50E-HT, Tanaka Kikinzoku Kogyo) and ionomer (Nafion D2020 and D1020, DuPont) were used for the cathode catalyst layers. The ionomer/carbon weight ratio was fixed in this study, because the main objective was to investigate the effect of solvent composition on the microstructure of the catalyst inks and catalyst layers. Table 2 shows the preparation conditions of the cathode catalyst ink. Solvents consisted of ultrapure water (Milli-Q, Millipore) and 1-propyl alcohol (NPA), and the weight ratio of water/NPA was 2:8, 6:4, and 10:0. The electrocatalyst and the ionomer were separately mixed and ground by a bead mill machine under the same conditions to prepare the catalyst inks. Then, a small amount of the ink was sampled to observe its microstructure and particle-size distribution, as explained below. The remaining inks were applied onto the membranes directly and dried to form the cathode catalyst layers by a pulse spray coating

	Cathode	Anode
electrocatalyst	TEC10E50E-HT (TKK)	Pt/GC (30 wt %)
ionomer	Nafion D2020 or D1020	Nafion D2020
Pt loading [$\text{mg}_\text{Pt}\cdot\text{cm}^{-2}$]	0.1	0.05
ionomer/carbon [w/w]	0.9	1.3
membrane	perfluorosulfonic acid type membrane	
gas diffusion layer	carbon paper type with microporous layer	
active area [cm^2]	10 (5×2)	

solvent	ultrapure water, 1-propyl alcohol (NPA)
water/NPA weight ratio	2:8, 6:4, 10:0
solid content of ink [wt %]	7
mixing media	bead mill (zirconia bead, $d = 1.5$ mm, Aimex)
mixing conditions	1500 rpm, 10 min
deposition media	pulse spray coating system (Nordson)
drying conditions	353 K, 15 min

method. A cross section of the catalyst layers was prepared and observed by typical scanning electron microscopy (SEM).

Analysis of Catalyst Ink Microstructure

The microstructure of the catalyst ink was analyzed by two methods: cryogenic scanning electron microscopy and laser diffraction.

Cryogenic Scanning Electron Microscopy (cryo-SEM)

A cryogenic scanning electron microscope (S-4800, Hitachi) equipped with a cryogenic stage (Alto2500, Gatan) was used to observe the microstructure of the “real” catalyst ink, typically used for coating process analysis and biological observation.^[35–38] The cryogenic stage was cooled below 173 K by gasified nitrogen from liquid nitrogen. The procedure used to observe the catalyst ink structure by cryo-SEM was as follows. For rapid freezing, a typical “metal contact method” was applied.^[37] First, the catalyst ink was put on the specimen holder of the cryo-SEM, whereas a copper block was partially soaked in liquid nitrogen for cooling. When the temperature of the copper block was low enough, the ink on the holder was pressed onto the plate and then soaked in liquid nitrogen. After this freezing process, the catalyst ink on the specimen holder was set on the cryogenic stage and inserted into the specimen chamber of the scanning electron microscope. Due to the low saturated vapor pressure at the low pressure in the specimen chamber of the scanning electron microscope, it was easy to sublimate the solvent of the frozen catalyst ink by slightly increasing the temperature. After removing the solvent from the frozen catalyst ink, the sublimated microstructure in the vicinity of the surface of the ink was observed by cryo-SEM.

Laser Diffraction

The microstructure of the catalyst ink was characterized by using a laser diffraction particle size analyzer (MT3000II, MicrotracBEL). The three catalyst inks of the cathode catalyst layers were diluted with 2-propyl alcohol (IPA) to less than 1 wt % of the solid content. Then, the particle-size distribution of each ink was measured promptly.

Characterization of Catalyst Layer Performance and Properties

The cathode catalyst layers prepared with different ink compositions were characterized as MEAs. First, the I - V performance was measured under the typical conditions given in Table 3, while measuring the high-frequency resistance at 1 kHz for iR correction. Second, to validate the I - V performance, the apparent electrochemical properties of the cathode catalyst layers were characterized. Cyclic voltammetry and linear sweep voltammetry were conducted to determine the electrochemical surface area (ECA) of the catalyst layers and crossover current.^[39] The ORR area-specific activity was defined at the iR -corrected 0.9 V versus RHE under a fully humidified oxygen atmosphere.^[39] Oxygen and proton-transport resistances of the cathode catalyst layers were analytically measured by limiting current and electrochemical impedance spectroscopy (EIS) measurements, respectively.^[12,13,17] The test conditions are shown in Tables 4 and 5. To project the oxygen-transport resistance in the cathode catalyst layer, the resistance in the microporous layer of the gas diffusion layer was measured and subtracted beforehand ($= 7 \text{ s m}^{-1}$). The cathode potential at which an ORR lim-

Table 3. Conditions for <i>I</i> - <i>V</i> performance measurements.		
	Anode	Cathode
cell temperature [K]		353
gas pressure [kPa_abs.]		200
reactant gas	H ₂	air
gas flow rate [N m ³ s ⁻¹]	6.7 × 10 ⁻⁵	2.5 × 10 ⁻⁴
relative humidity [%]		90
hold time at each current [s]		300

Table 4. Conditions for oxygen-transport resistance measurement in the cathode catalyst layer. ^[12,13]		
	Anode	Cathode
cell temperature [K]		353
gas pressure [kPa_abs.]		108, 130, 154, 202
reactant gas	H ₂	diluted O ₂ with N ₂
gas flow rate [N m ³ s ⁻¹]	6.7 × 10 ⁻⁵	2.5 × 10 ⁻⁴
O ₂ concentration [%]	-	1.0, 1.3, 1.8, 2.6
relative humidity [%]		90
cathode potential [V vs. RHE]		≈ 0.2

Table 5. Conditions for EIS measurements. ^[17]		
	Anode (CE, RE) ^[a]	Cathode (WE) ^[a]
cell temperature [K]		353
gas pressure [kPa_abs.]		100
reactant gas	H ₂	N ₂
gas flow rate [N m ³ s ⁻¹]		8.3 × 10 ⁻⁶
relative humidity [%]		100, 40
frequency [Hz]		15 000–0.1
amplitude [mV]		15
WE potential bias [V vs. RHE]		0.45

[a] CE = counter electrode, RE = reference electrode, WE = working electrode.

iting current was observed was confirmed in advance (≈ 0.2 V vs. RHE). Finally, the correlation was analyzed among the *I*-*V* performance, electrochemical properties, and microstructure of the catalyst layers and the catalyst ink.

2. Results and Discussion

2.1. Observation of Catalyst Ink Structure by Cryo-SEM and Laser Diffraction

Figure 1 shows a typical cryo-SEM image of the catalyst ink structure at water/NPA = 6:4. Some agglomerates of the platinum-loaded carbon (Pt/C) electrocatalyst surrounded by an ionomer network are observed. Regarding the agglomerates of the Pt/C electrocatalyst, two sizes of the agglomerates, large and small, are clearly observed. On the other hand, the ionomer structure around the agglomerates looks like a spider's web, maybe affected by the rate of formation of ice crystals during freezing.^[37]

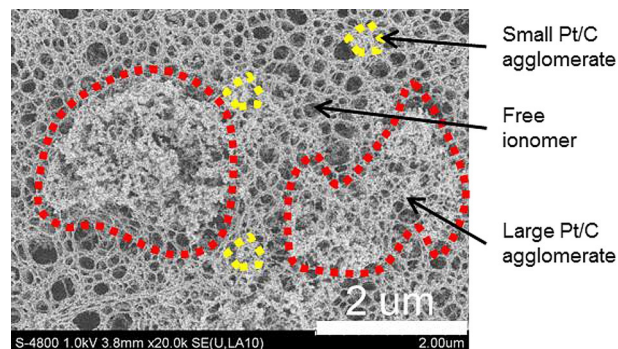


Figure 1. Typical cryo-SEM image of the catalyst ink structure at a water/NPA weight ratio of 6:4.

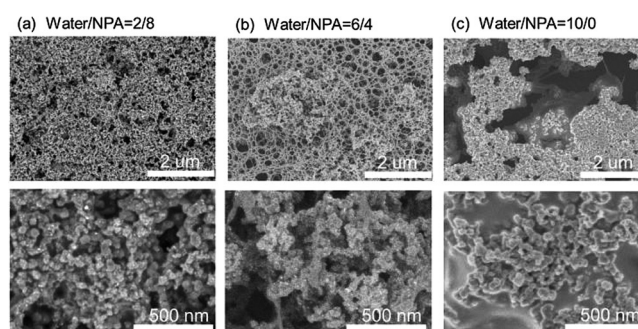


Figure 2. Comparison of the catalyst ink structure at a water/NPA weight ratio of a) 2:8, b) 6:4, and c) 10:0.

Figure 2 shows a comparison of the catalyst ink structure at different water/NPA weight ratios. Good dispersion of Pt/C and the ionomer in the catalyst ink is observed at water/NPA = 2:8 in Figure 2a. According to the more microscopic image in Figure 2a, the ionomer might cover the Pt/C agglomerate well, as if it were an actual catalyst layer. On the other hand, increasing the water weight fraction in the solvent can increase the size of the agglomerate, and phase segregation of the Pt/C and ionomer is clearly observed at water/NPA = 10:0 in Figure 2c. The ionomer distribution in the ink is heterogeneous. Some portions of the ink have much more ionomer, whereas other portions have less. Furthermore, large voids made from solvent sublimation are observed.

The above phenomena can be interpreted by fundamental studies. Theoretical analyses indicate that if there is much alcohol in the solvent, the molecular structure of the Nafion ionomer is well expanded and the carbon particles are dispersed due to hydrophobic interactions among the methyl group of the alcohol, the fluorocarbon-based ionomer backbone, and the hydrophobic carbon surface.^[40,41] On the other hand, it was experimentally observed that the Nafion ionomer can form aggregates in water-rich solvents.^[29,42] This is also consistent with the theoretical studies,^[40,41] that is, the ionomer can easily form an aggregate because the fluorocarbon backbone does not have much interaction with the water molecules but interacts more with itself.

To validate the different sizes of the agglomerates, the particle-size distribution of the three catalyst inks was measured by

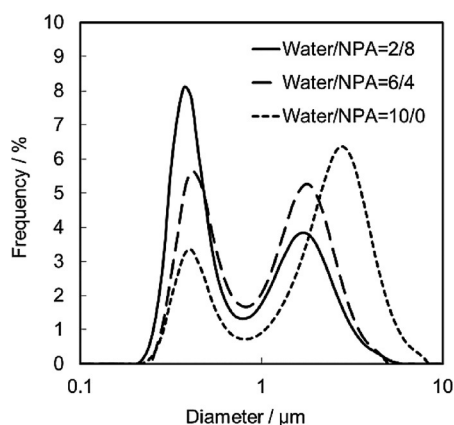


Figure 3. Particle-size distribution of the three catalyst inks (Pt/C with ionomer, water/NPA = 2:8, 6:4, 10:0).

laser diffraction, as shown in Figure 3. Although the solid content of the measured ink by laser diffraction was diluted relative to that of the “real” catalyst inks, it was shown that each ink has bimodal spectra. If the alcohol content in the solvent is high, the peak corresponding to the smaller particle size is more significant than the other. In the case of a water-rich ink (water/NPA = 10:0), the mean diameter above 1 μm is shifted and becomes remarkably larger. To understand the bimodal peaks further, one additional ink of Pt/C without the ionomer was prepared by keeping the other conditions the same. Figure 4 shows the comparison of the two inks with and without the ionomer. It is clearly observed that the smaller peak of the bimodal spectrum is significantly decreased without the ionomer relative to that with the ionomer, which indicates that small Pt/C agglomerates with submicron mean diameters might be covered with the ionomer.

These results are consistent with those of the cryo-SEM qualitative observations. If the catalyst ink is alcohol rich, the Pt/C agglomerates can be relatively small, well dispersed, and covered with more of the ionomer. On the contrary, the Pt/C agglomerates become larger and tend to segregate from the ionomer in a water-rich catalyst ink. According to previous research efforts, the optimum catalyst ink can be obtained from

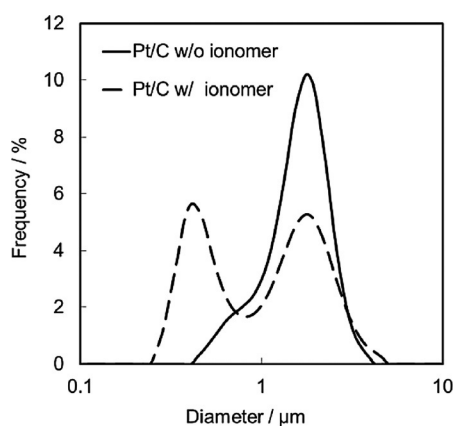


Figure 4. Comparison of the particle-size distributions of the catalyst inks (Pt/C with and without ionomer, water/NPA = 6:4).

a water/alcohol mixture, and 100% of either a water- or alcohol-based solvent does not provide a well-dispersed catalyst ink.^[28,30,43] Our results at water/NPA = 10:0 show remarkable phase segregation, which is indicative of good agreement with the results already published.

2.2. Characterization of Cathode Catalyst Layers

2.2.1. Cross Section of Cathode Catalyst Layers

The three catalyst inks with different water/NPA weight ratio were separately deposited on the membranes to form cathode catalyst layers. Figure 5 shows typical cross sections of the

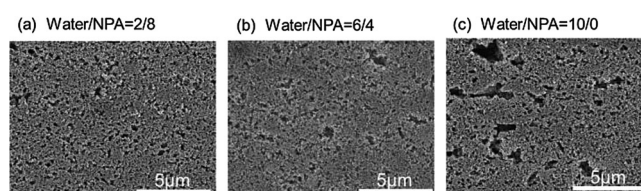


Figure 5. Cross section of cathode catalyst layers at a water/NPA weight ratio of a) 2:8, b) 6:4, and c) 10:0.

three catalyst layers. The images of the catalyst layer structure show qualitative agreement with those of the catalyst inks in Figure 2. The secondary pores of the catalyst layer in between the agglomerates seem small in the NPA-rich case (water/NPA = 2:8), whereas large pores are observed in the water-rich case (water/NPA = 10:0). Besides, the thickness of the three catalyst layers is almost the same.

Regarding a more microscopic structure, Park et al. investigated ionomer morphology on a platinum-based electrocatalyst (platinum nanoparticles on graphitized carbon black).^[43] They mentioned that the ionomer with a high ion-exchange capacity (IEC, 1.43 meq g⁻¹) and a short side chain covered the electrocatalyst more uniformly than an ionomer with a normal IEC (0.99 meq g⁻¹) and long side chains. Because sulfonic acid groups interact with water more than alcohols, an ionomer with a high IEC is well dispersed. In our study, the catalyst ink with no alcohol (water/NPA = 10:0) and the normal Nafion ionomer is consistent with their results. Discussion of the ionomer distribution in the through-plane direction is given in Section 2.2.5.

2.2.2. I–V Performance

Figure 6 shows the *iR*-free *I*–*V* performance of the MEAs by applying the three catalyst inks to the cathode catalyst layers. In the low current density region such as around 0.1 A cm⁻², mainly dominated by ORR kinetic properties, the MEA from the water-rich ink (water/NPA = 10:0) shows the best performance of the three catalysts. On the other hand, a voltage drop is observed in the water-rich case at a high current density (e.g. 2.0 A cm⁻²), mainly governed by mass-transport properties, and the MEA with the water/NPA = 6:4 ink shows the best per-

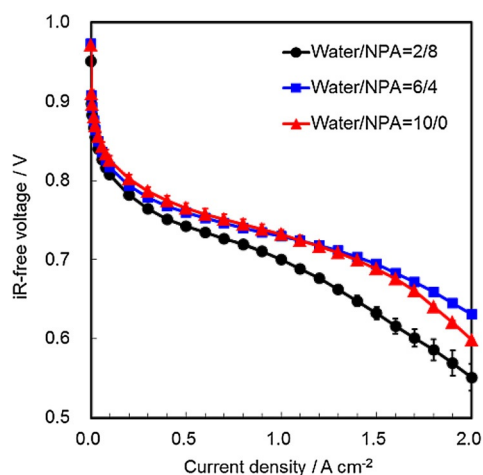


Figure 6. *iR*-free *I*-*V* performance of the MEAs by applying three different catalyst inks to the cathode catalyst layers.

formance. As shown in Figure 5, the larger pores are increased at water/NPA = 10:0, and a Nafion ionomer with a normal equivalent weight (EW = 1000) was used in this study. Therefore, it is considered that the hydrophobic large pores might be increased at water/NPA = 10:0, and this would result in water accumulation and flooding. The MEA from the water/NPA = 2:8 ink exhibits low performance as a whole under these conditions. For further validation of the *I*-*V* performance, ORR kinetics and mass-transport properties of the catalyst layers will be investigated and discussed at a later date.

2.2.3. ORR Kinetic Properties

Figure 7 shows the ORR kinetic properties. Figure 7a denotes the ORR area-specific activity, the current density at 0.9 V divided by ECA shown in Figure 7b. If the cathode catalyst ink is water rich, the apparent ORR area-specific activity of the MEA significantly increases. Many researchers have indicated that the ionomer is adsorbed on the platinum surface even under aqueous measurement conditions^[44–48] and is likely to suppress the adsorption of oxygen molecules on the platinum surface.^[45,47] Related to the phenomenon, it was reported that ionomer coverage on platinum can have a negative impact on the apparent ORR area-specific activity.^[22] Therefore, it is considered that the ionomer can cover the surface of the electrocatalyst in the alcohol-rich case more than in the water-rich case, which probably originates from a more dispersed ionomer structure in the alcohol-rich catalyst ink in this study.

On the other hand, the ECA slightly increases with the water content in the catalyst ink, even though the ionomer coverage on the electrocatalyst probably decreases. Eikerling pointed out that water can act as a proton conductor in the nano-scale.^[49,50] Therefore, a proton can be underpotentially adsorbed to be a hydrogen atom on the platinum surface through the water network, which results in the adequate ECA value. These kinetic properties might affect the *I*-*V* performance, especially in the low current density region.

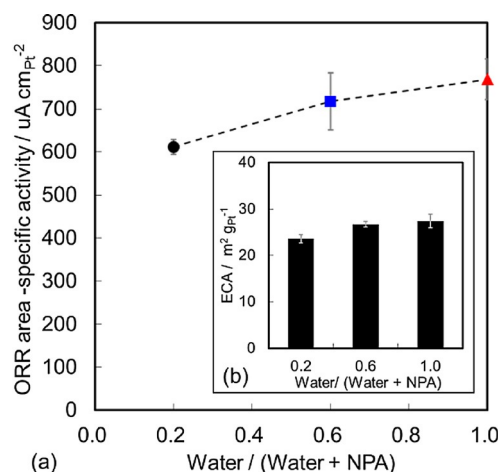


Figure 7. ORR kinetic properties of the MEAs by applying three different catalyst inks to the cathode catalyst layers. a) ORR area-specific activity of the MEAs. b) Comparison of the electrochemical surface areas (ECAs).

2.2.4. Oxygen Transport Resistance in Cathode Catalyst Layers

Figure 8 shows the projected oxygen-transport resistance in cathode catalyst layers fabricated from the three different catalyst inks. Interestingly, the oxygen-transport resistance shows a minimum value of the three at water/NPA = 6:4, whereas the alcohol-rich case (water/NPA = 2:8) shows the largest oxygen-transport resistance value.

Toyota, General Motors, and Nissan have suggested that the gas-transport resistance obtained from this technique can include resistance in the ionomer surrounding the electrocatalyst.^[11,13–16] Furthermore, because the cathode platinum loading is $0.1 \text{ mg}_{\text{Pt}} \text{ cm}^{-2}$ in this study, the resistance in the ionomer might be preferentially evaluated.^[11,13–16] As a result, it is likely that the ionomer can cover the electrocatalyst in the alcohol-rich case more than in the water-rich case. This can result in a larger oxygen-transport resistance in the alcohol-rich case, because oxygen must go through the ionomer. On the other

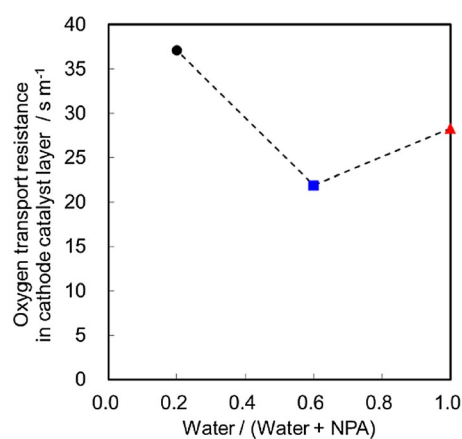


Figure 8. Projected oxygen-transport resistance in the cathode catalyst layers of the MEAs by applying three different catalyst inks to the cathode catalyst layers.

hand, hydrophobic large pores can yield flooding in the water-rich case, as mentioned in Section 2.2.2. Therefore, oxygen would not necessarily penetrate the ionomer and go directly into the agglomerate, but it has less impact on the transport resistance than in the alcohol-rich case. Besides, because the size of the agglomerate becomes significantly larger, as shown in Figure 3, the transport distance inside the agglomerate might be longer than that of the NPA-rich case.

2.2.5. Proton-Transport Resistance in Cathode Catalyst Layers

Figure 9 shows typical Nyquist plots of the cathode catalyst layers from the three different inks under 100 and 40% relative humidity conditions. Proton-transport resistance in the membrane was already subtracted from the experimental data. Apparent proton-transport resistance in the cathode catalyst layer is estimated from the intercept of the x axis and the extrapolated line from the data in the low-frequency region.^[17,18]

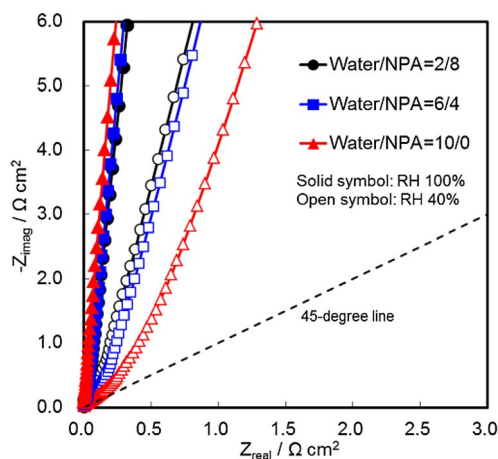


Figure 9. Typical Nyquist plots of the MEAs by applying three different catalyst inks to the cathode catalyst layers.

Under fully humidified conditions, the Nyquist plots of the three inks are similar, and the apparent proton-transport resistance at water/NPA = 10:0 is the smallest of the three. In addition, the slopes around the high-frequency region are steeper than 45°. On the other hand, the largest transport resistance occurs at water/NPA = 10:0 under the dry conditions with a 45° slope. The other cases indicate smaller apparent proton-transport resistance and maintain the steep slopes.

As shown in Figure 2, there is larger ionomer phase in the water-rich case. However, as described above, the apparent proton-transport resistance of the catalyst layer at water/NPA = 10:0 is the largest under the dry conditions. This tricky trend might be attributed to the large ionomer phase and adsorbed water in the catalyst layer, which can act as a proton conductor.^[49,50] Water can exist inside the large agglomerates so that it may compensate for proton transport inside. Regarding the ionomer network itself, the catalyst layer from the water-rich catalyst ink forms poor ionomer connectivity and has low coverage on large agglomerates of the electrocatalyst, whereas

that from the NPA-rich ink can form a well-connected ionomer network in terms of percolation.^[50,51] In addition, according to the transmission model, steep slopes more than 45° can indicate a decreasing local proton-transport resistance in the through-plane direction of the catalyst layer toward the membrane side.^[17,18] This can be attributed to direct-spray coating onto the membrane used in this study. Previous studies suggest that some free ionomer could exist in the inks not adsorbed on the electrocatalyst^[32,34] and that it can settle down easily toward the membrane direction if the ink is applied onto the membrane and dried.^[52,53] Besides, it was also indicated that the ionomer tends to detach from the electrocatalyst if the catalyst ink is alcohol rich because of more interaction between the alcohol and the backbone of the ionomer.^[40,41] This can be the cause of the uneven distribution of the ionomer, which results in the steep slope at water/NPA = 2:8 and 6:4 under the dry conditions.

Consequently, the above interpretation of the oxygen- and proton-transport properties and the microstructure of the catalyst layers can qualitatively explain the I - V performance in the high-current density region.

2.3. Proposed Microstructure of Catalyst Ink/Catalyst Layer and Relationship with Electrochemical Properties

According to the above discussion on the structure and properties, we proposed microstructures of the catalyst ink and catalyst layer with reference to the electrochemical properties, as shown in Figure 10. If there is much alcohol (water/NPA = 2:8 in this study) in the catalyst ink, small and dispersed Pt/C agglomerates tend to form with a relatively high ionomer coverage on the agglomerate in the ink. That can yield a macro-homogeneous catalyst layer structure with small agglomerates and pores and a high ionomer coverage. Therefore, the catalyst layer is well packed, shows good ionomer connectivity, low apparent ORR area-specific activity, and high oxygen-transport resistance even though the agglomerate size is small.

Water/NPA	2/8	6/4	10/0
Catalyst Ink	<ul style="list-style-type: none"> • More small agglomerate • Less free ionomer between agglomerate 	<ul style="list-style-type: none"> • Mixed size agglomerate • Free ionomer between agglomerate 	<ul style="list-style-type: none"> • More large agglomerates • More free ionomer between agglomerate
Catalyst Layer	<ul style="list-style-type: none"> • Small agglomerate size • Macro homogenous and high ionomer coverage 	<ul style="list-style-type: none"> • Middle agglomerate size • Partial ionomer coverage 	<ul style="list-style-type: none"> • Large agglomerate size • Heterogeneous and low ionomer coverage with water

Figure 10. Proposed microstructure of the catalyst ink/catalyst layer and relationship with electrochemical properties.

On the other hand, in the case of water-rich conditions (water/NPA = 10:0 in this study), large Pt/C agglomerates and phase segregation of Pt/C and the ionomer is observed, and a self-organizing free ionomer can exist between the Pt/C agglomerates. Then, the catalyst layer has large secondary pores. It may have heterogeneous and small ionomer coverage on the large Pt/C agglomerates with water. This can result in better ORR area-specific activity, worse ionomer network, better proton transport under wet conditions, and a larger oxygen-transport resistance relative to the intermediate case with water/NPA = 6:4. This intermediate case is optimum in this study from the points of view of performance and properties, because the sizes of the Pt/C agglomerates and pores and the ionomer coverage on the Pt/C agglomerates may be suitable, which is indicative of good I - V performance, ORR kinetics, and mass-transport properties.

As a result, the above scenario associated with the microstructure and the electrochemical properties can explain differences in the I - V performance in Figure 6. Besides, the catalyst layers show structural analogy to the catalyst inks. Therefore, the catalyst ink has a strong impact on the formation of the structure of the catalyst layer and thus plays an important role in performance.

3. Conclusions

We tried to understand the formation of the microstructure of a catalyst layer by using the "real" catalyst ink, an intermediate state from the consisting materials to the formation of the catalyst layer. First, cryogenic scanning electron microscopy (cryo-SEM) was applied to observe the structure of the catalyst ink, and it was successfully visualized. According to the cryo-SEM images of catalyst inks with three different water/1-propyl alcohol ratios, the size of the agglomerates of the Pt/C electrocatalyst changed. If there was much alcohol in the catalyst ink, the number of small agglomerates increased. The ionomer was likely to be dispersed and to cover the agglomerate well. In contrast, in the case of a water-rich catalyst ink, the size of the agglomerate increased and segregation between the agglomerate and the ionomer was remarkable. Laser diffraction also indicated that each ink had a bimodal particle-size distribution, and the frequency of the two peaks could be changed with the water/alcohol ratio of the ink. Second, catalyst layers were formed from the three inks and their cross sections were observed by SEM, which indicated a trend similar to the structure of the catalyst inks.

Then, electrochemical characterization, such as current-voltage (I - V) performance, oxygen reduction reaction kinetics, and mass-transport properties, was conducted to understand the I - V performance and the microstructure of the ionomer around the electrocatalyst. The electrochemical properties suggested an ionomer microstructure around the Pt/C agglomerates in the catalyst layers, and a qualitative relationship was revealed from the catalyst materials on the performance of the cathode catalyst layer of the membrane electrode assembly through formation of the microstructure and its apparent

properties. It was also found that the microstructure of the catalyst ink plays an important role in performance.

Acknowledgements

The authors gratefully acknowledge fruitful discussions with Professor A. Miyazawa, Professor Y. Nishino (University of Hyogo), and Dr. Y. Ito (Leica-microsystems) on the cryo-SEM technique and its interpretation.

Keywords: catalyst layer · fuel cells · inks · microporous materials · polymers

- [1] C. Chen, Y. Kang, Z. Huo, Z. Zhu, W. Huang, H. L. Xin, J. D. Snyder, D. Li, J. A. Herron, M. Mavrikakis, M. Chi, K. L. More, Y. Li, N. M. Markovic, G. A. Somorjai, P. Yang, V. R. Stamenkovic, *Science* **2014**, *343*, 1339–1343.
- [2] R. R. Adzic, *Electrocatalysis* **2012**, *3*, 163–169.
- [3] S. M. Alia, K. Jensen, C. Contreras, F. Garzon, B. Pivovar, Y. Yan, *ACS Catal.* **2013**, *3*, 358–362.
- [4] A. B. Papandrew, R. W. Atkinson III, G. A. Goenaga, S. S. Kocha, J. W. Zack, B. S. Pivovar, T. A. Zawodzinski Jr., *J. Electrochem. Soc.* **2013**, *160*, F848–F852.
- [5] H. Yano, T. Akiyama, M. Watanabe, H. Uchida, *J. Electroanal. Chem.* **2013**, *688*, 137–142.
- [6] H. Daimon, M. Inaba, *Electrochemistry* **2013**, *81*, 641645.
- [7] A. Ishihara, M. Tamura, Y. Ohgi, M. Matsumoto, K. Matsuzawa, S. Mitsuhashi, H. Imai, K. Ota, *J. Phys. Chem. C* **2013**, *117*, 18837–18844.
- [8] B. Arumugam, B. A. Kakade, T. Tamaki, M. Arao, H. Imai, T. Yamaguchi, *RSC Adv.* **2014**, *4*, 27510–27517.
- [9] K. L. More, *Characterization of Fuel Cell Materials*, Proceeding of 2014 DOE Annual Merit Review, June 2014, Washington, DC.
- [10] T. Ito, U. Matsuwaki, Y. Otsuka, M. Hatta, K. Hayakawa, K. Matsutani, T. Tada, H. Jinnai, *Electrochemistry* **2011**, *79*, 374–376.
- [11] A. Ohma, T. Mashio, K. Sato, H. Iden, Y. Ono, K. Sakai, K. Akizuki, S. Takai-chi, K. Shinohara, *Electrochim. Acta* **2011**, *56*, 10832–10841.
- [12] T. Mashio, A. Ohma, S. Yamamoto, K. Shinohara, *ECS Trans.* **2007**, *11*, 529–540.
- [13] K. Sakai, K. Sato, T. Mashio, A. Ohma, K. Yamaguchi, K. Shinohara, *ECS Trans.* **2009**, *25*, 1193–1201.
- [14] H. Iden, T. Mashio, A. Ohma, *J. Electroanal. Chem.* **2013**, *708*, 87–94.
- [15] N. Nonoyama, S. Okazaki, A. Z. Weber, Y. Ikogi, T. Yoshida, *J. Electrochem. Soc.* **2011**, *158*, B416–B423.
- [16] J. P. Owejan, J. E. Owejan, W. Gu, *J. Electrochem. Soc.* **2013**, *160*, F824–F833.
- [17] M. C. Lefebvre, R. B. Martin, P. G. Pickup, *Electrochem. Solid-State Lett.* **1999**, *2*, 259–261.
- [18] R. Makharia, M. F. Mathias, D. R. Baker, *J. Electrochem. Soc.* **2005**, *152*, A970–A977.
- [19] H. Iden, A. Ohma, K. Shinohara, *J. Electrochem. Soc.* **2009**, *156*, B1078–B1084.
- [20] H. Iden, K. Sato, A. Ohma, K. Shinohara, *J. Electrochem. Soc.* **2011**, *158*, B987–B994.
- [21] H. Iden, A. Ohma, *J. Electroanal. Chem.* **2013**, *693*, 34–41.
- [22] Y. Furuya, H. Iden, T. Mashio, A. Ohma, K. Shinohara, *221st ECS Meeting Abst.* **2012**, 1522.
- [23] M. Uchida, Y. Aoyama, N. Eda, A. Ohta, *J. Electrochem. Soc.* **1995**, *142*, 463–468.
- [24] M. Uchida, Y. Fukuoka, Y. Sugawara, H. Ohara, A. Ohta, *J. Electrochem. Soc.* **1998**, *145*, 3708–3712.
- [25] S. Shin, J. Lee, H. Ha, S. Hong, H. Chun, I. Oh, *J. Power Sources* **2002**, *106*, 146–152.
- [26] R. Fernández, P. Ferreira-Aparicio, L. Daza, *J. Power Sources* **2005**, *151*, 18–24.
- [27] Z. Xie, X. Zhao, M. Adachi, S. Ken, T. Mashio, A. Ohma, K. Shinohara, S. Holdcroft, T. Navessin, *Energy Environ. Sci.* **2008**, *1*, 184–193.
- [28] C. M. Johnston, K. S. Lee, T. Rockward, A. Labouriau, N. Mack, Y. S. Kim, *ECS Trans.* **2009**, *25*, 1617–1622.

- [29] T. T. Ngo, T. L. Yu, H.-L. Lin, *J. Power Sources* **2013**, *225*, 293–303.
- [30] D. Huang, P. Yu, F. Liu, S. Huang, K. Hsueh, Y. Chen, C. Wu, W. Chang, F. Tsau, *Int. J. Electrochem. Sci.* **2011**, *6*, 2551–2565.
- [31] A. Strong, B. Britton, D. Edwards, T. J. Peckham, H. Lee, W. Y. Huang, S. Holdcroft, *J. Electrochem. Soc.* **2015**, *162*, F513–F518.
- [32] S. Ma, Q. Chen, F. H. Jørgensen, P. C. Stein, E. M. Skou, *Solid State Ionics* **2007**, *178*, 1568–1575.
- [33] F. Xu, H. Y. Zhang, J. Ilavsky, L. Stanciu, D. Ho, M. J. Justice, H. I. Petrache, J. Xie, *Langmuir* **2010**, *26*, 19199–19208.
- [34] M. Shibayama, T. Matsunaga, T. Kusano, K. Amemiya, N. Kobayashi, T. Yoshida, *J. Appl. Polym. Sci.* **2014**, *131*, 39841.
- [35] S. S. Prakash, L. F. Francis, L. E. Scriven, *J. Membr. Sci.* **2006**, *283*, 328–338.
- [36] H. Luo, L. E. Scriven, L. F. Francis, *J. Colloid Interface Sci.* **2007**, *316*, 500–509.
- [37] http://www.jeol.co.jp/en/applications/pdf/sm/469_en.pdf.
- [38] Y. Nishino, Y. Ito, A. Miyazawa, *Advantages of Cryo-scanning Electron Microscopy for Biological Specimens*, 2013, JSM-BA Seminar, Jupiter, USA.
- [39] A. Iiyama, K. Shinohara, A. Ohma, T. Yoshida, A. Daimaru, *Objectives, R&D Challenge Topics and Proposed Evaluation Methods for Polymer Electrolyte Fuel Cells* **2011**, FCCJ.
- [40] K. Malek, M. Eikerling, Q. Wang, T. Navessin, Z. Liu, *J. Phys. Chem. C* **2007**, *111*, 13627–13634.
- [41] T. Mashio, A. Ohma, T. Tokumasu, *Molecular Dynamics Study of Ionomer Structure Formation in Catalyst Ink*, 65th ISE meeting, Lausanne, Switzerland, **2014**.
- [42] C. A. Cleveland, M. Hickner, J. E. McGrath, *Effect of Solvent Composition and Concentration on Aggregate Size in Polymer Dispersions for Fuel Cell Membrane Electrode Assembly*, **2010**.
- [43] Y.-C. Park, K. Kakinuma, H. Uchida, M. Watanabe, M. Uchida, *J. Power Sources* **2015**, *275*, 384–391.
- [44] R. Subbaraman, D. Strmcnik, V. Stamenkovic, N. M. Markovic, *J. Phys. Chem. C* **2010**, *114*, 8414–8422.
- [45] A. Ohma, K. Fushinobu, K. Okazaki, *Electrochim. Acta* **2010**, *55*, 8829–8838.
- [46] T. Masuda, F. Sonsudin, P. R. Singh, H. Naohara, K. Uosaki, *J. Phys. Chem. C* **2013**, *117*, 15704–15709.
- [47] K. Kodama, A. Shinohara, N. Hasegawa, K. Shinozaki, R. Jinnouchi, T. Suzuki, T. Hatanaka, Y. Morimoto, *J. Electrochem. Soc.* **2014**, *161*, F649–F652.
- [48] J. Omura, H. Yano, M. Watanabe, H. Uchida, *Langmuir* **2011**, *27*, 6464–6470.
- [49] Q. Wang, M. Eikerling, D. Song, Z. Liu, *J. Electroanal. Chem.* **2004**, *573*, 61–69.
- [50] M. Eikerling, *J. Electrochem. Soc.* **2006**, *153*, E58–E70.
- [51] Y. Liu, M. W. Murphy, D. R. Baker, W. Gu, C. Ji, J. Jorne, H. A. Gasteiger, *J. Electrochem. Soc.* **2009**, *156*, B970–B980.
- [52] S. S. Prakash, L. F. Francis, L. E. Scriven, *J. Membr. Sci.* **2008**, *313*, 135–157.
- [53] F. Buss, C. C. Roberts, K. S. Crawford, K. Peters, L. F. Francis, *J. Colloid Interface Sci.* **2011**, *359*, 112–120.

 Manuscript received: March 30, 2015

Revised: May 19, 2015

Final Article published: July 14, 2015